State of the art experimental apparatus for fast entangling gates in trapped multi-ion crystals

Donovan Webb

Department of Physics, University of Oxford

E-mail: donovan.webb@physics.ox.ac.uk

Abstract.

Scalable trapped-ion quantum computation relies on the development of high-fidelity fast entangling gates in many ion crystals. Currently the speed of geometric phase gates are limited by either large scattering errors (with Raman transitions) or off-resonant carrier excitations (with quadrupole transitions). Utilizing standing waves offers a potential pathway to achieve fast entanglement in quadrupole transitions due to suppressing undesired carrier excitations. Using a legacy apparatus we present initial results of this carrier suppression in the 674 nm quadropole transition of $^{88}Sr^{+}$. We demonstrate fast two-qubit entangling gates which exceed the entangling "speed limit" imposed by off resonant carrier excitations. To explore these "fast gates" at durations comparable to the secular trap frequency, and in multi-ion chains, a new system is been constructed. This system will use a segmented 3D Paul trap for greater control of long ion chains, and will feature single ion addressing for both selective and high power coherent operations. We present the current progress and roadmap of this next-generation platform and motivations behind design choices.

1. Introduction

*Trapped Ion QC
General idea of spin coupled with HO
*Entangling gates MS gate
*Non-Adiabatic interactions
*Fast Gate Schemes

Previously the physicist was limited to thought experiments on the Quantum nature of single particles. It was inconceivable to isolate, probe and entangle together single particles. However the advent of Ion traps, specifically Paul and Penning traps, have enabled the experimental exploration and corroboration of Atomic theory producing incredibly precise measurements such as XXclocks, relativity, g factorXX [clocks, relativity, g factor].

With the high degree of experimental control of a quantum system exhiibited by Ion trap systems, they are an obvious and increasingly mature platform for enabling Quantum Computation.

Ion-traps trap ions through a combination of static and oscillating electric fields. Ions will sit at local minima of this potential and experience harmonic motion. When N ions are trapped simultaneously they may form linear strings or crystals due to the combination of trapping potential and mutual repulsion between like charged ions. A linear crystal of N ions will exhibit $3N$ normal modes. These single ions within the crystal may be modelled as two level "spin" systems, whilst the harmonic motion is modelled as a "spring" system. We may utilize the shared motion of ions to entangle their spin states.

Describe entangling... With Lamb-Dicke approximation: H = Carrier + eta*SB

Controlled light-matter interactions are essential for quantum computing [1–3], quantum simulation [4, 5], and metrology [6, 7]

********** From paper **********

For trapped ions, controlled light-matter interactions typically require carrier interactions that only couple the internal qubit states, as well as sideband interactions that couple these internal states to their collective motion [3]. For example, the sideband interactions, driven by the spatial gradient of the carrier coupling, are used to mediate spin-spin interactions such as entangling gates [8]. Conventionally, coherent control of laser-ion interactions is achieved using traveling waves (TWs) [3]. As the ions experience an averaged electric field and gradient over the interaction duration, the ratio between carrier coupling and sideband coupling is fixed. In contrast, the coupling strengths for ions in a standing wave (SW) vary with the spatial structure of the light field along the propagation direction. Consequently, the phase of the SW at the ions sets the ratio between the carrier and the sideband coupling. Coherent SW interactions on a single ion have been studied previously using cavities [9, 10], integrated optics [11] and free-space approaches [12]. However, coherent operations on multiple ions with a SW have so far been unexplored.

The tunability of the carrier:sideband coupling ratio is especially important for strong interactions where off-resonant terms start participating significantly and cannot be eliminated adiabatically. For example, in the conventional Mølmer Sørensen (MS) mechanism [13], the TW that generates the spin-motion coupling also gives rise to an off-resonant carrier coupling, which causes an error in the entangling operation. This error becomes significant as the carrier interaction strength approaches the motional frequency, placing a limit on the speed of the entangling operation. Using a SW instead enables high-fidelity entangling operations that can surpass this speed limit by selectively enhancing the spin-motion coupling while coherently suppressing the detrimental carrier term [14].

We show that the presence of the carrier coupling term, in the context of the TW-MS gate, leads to a reduction in the spin-dependent force (SDF) magnitude, which scales with the Rabi frequency of this detrimental term, posing an inherent speed limit

for this mechanism.

It can be shown that a travelling wave MS in the interaction picture obeys equation 4 of paper, where the SDF follows a bessel like relationship as shown in fig X, featuring a global maximum achievable force amplitude. This maximum point direclty limits the speed at which gates can be achieved.
****

2. Carrier Nulling Results

Excerpts from carrier nulling paper kind of want to put this after the FG description... Or could I shorten this massively to reduce emphasis?

As discussed in sectionXX, the use of phase-stable standing waves (SW) is a clear route to fast entangling gates on quadrupole transition qubits. Here we report experimental results of both SW single qubit gates and SW Molmer Sorensen (MS) entangling gates performed on the Blade apparatus.

We use a free-space, phase-stabilized SW formed by two superimposed counter-propagating 674-nm beams that couple to the quadrupole qubit transition, 5S1/2 4D5/2, in 88Sr+.

**Here quadrupole so gradient couples carrier whilst XXCurlXX couples the sideband interaction

.

The single-qubit gate is created using a monochromatic SW on resonance with the qubit transition while placing the node(s) of the SW at the position of the ion(s). The two-qubit entangling gate is implemented via an MS-type scheme where we use a bichromatic SW instead of the conventional bichromatic TW.

Using the SW-MS instead, with the anti-nodes placed at the ions, we strongly suppress the undesired carrier term and show that we can surpass this speed limit.

**Look at poster for description of phase feedback onto the ion - maybe exclude this to shorten section.

still to tidy Results:
We probe the position of the SW relative to a single ion by applying a monochromatic SW pulse on resonance with the qubit transition [Figs. 1(b), 2(a)]. The pulse duration corresponds to a -pulse at maximum carrier coupling, which occurs at the nodes of the SW. For an electric quadrupole transition, the maximum carrier coupling occurs at the maximum gradient of the electric field [9]. We can maximize the carrier coupling and

minimize the sideband coupling, or vice versa, by selecting = or = 0 [Fig. 2(b)]. The transfer probability shown in Fig. 2(a) has a quartic dependence on near = and a quadratic dependence at = 0 [26]. When probing the suppressed motional sideband [Fig. 2(b) left], we observe only features that are due to the off-resonant (by 1.2 MHz) carrier coupling. By changing of the SW, we can realise any ratio between carrier and sideband coupling.

Expand this section and show some data of RBM results:
Furthermore, we perform randomized benchmarking [32] to evaluate the quality of single-qubit gates implemented using the SW and TW with the same duty cycle. We obtain an error of 1.44(3) × 10−3 and 1.73(3) × 10−3 per Clifford gate, respectively. Thus, use of the SW is not detrimental to single-qubit control.

We experimentally demonstrate two-qubit MS gates using a bichromatic TW for gate speeds in a regime where the carrier coupling induces a significant error which cannot be eliminated adiabatically. However, the bichromatic SW enables us to surpass this limit without degrading the fidelity (Fig. 4). To implement the SW-MS gate, we simultaneously suppress the carrier coupling on both ions by adjusting the ion spacing such that they are both placed at anti-nodes of the SW [Fig. 1(c)] [26]. We perform the TW and SW two-qubit entangling gates on the axial in-phase mode and optimize the experimental parameters to maximize the Bell-state fidelity for a fixed gate duration. In both cases, we use a ramp duration of 10 s to minimize coupling to the other motional modes [33]. This pulse ramping could be replaced with more sophisticated amplitude shaping techniques [16, 35]. In Fig. 4(a) we show the two-qubit fidelities achieved with the two schemes as a function of the effective gate duration (2 / g, where g = − z) [37]. For slower gates, the fidelity of the SW-MS is comparable with that of the TW-MS. For faster entangling gates, the fidelity of the TW-MS degrades rapidly. This is also predicted by direct numerical integration of Eq. (3); we set all the parameters to the experimental values except for the Rabi frequency Ω, which we optimize for maximum fidelity (dashed line). We also indicate the idealized case which neglects imperfect transfer into the interaction picture w.r.t. the carrier [Eq. (3)] (dotted line). We believe that the measured fidelities degrade sooner as a result of experimental imperfections (e.g. ramp shape) not captured by the numerical integration. In contrast, the fidelity for the SW-MS is consistent with 0.95 over the entire available power range, showing that we have eliminated the limit arising from the carrier coupling. The shortest SW-MS gate was 15 s, limited by the available total power of 29 mW.

*Shorten conclusion and change in such a way that focusses on what to improve/adapt in FG setup

In conclusion, we implemented single- and two-qubit operations for trapped-ion qubits using a phase-stabilized SW. Two counter-propagating beams create the SW,

whose relative phase at the ion position is stable to /100. This enabled us to tune the ratio of the field intensity and gradient that the ions experience, which sets the relative strengths of the sideband and carrier interactions. We use this new degree of control to suppress the unwanted off-resonant carrier coupling (by a factor of 18), while coherently enhancing the motional coupling during two-qubit gates. We show theoretically and experimentally that the non-commuting carrier term imposes a limit on the speed of conventional TW-MS gates, which were avoided using the SW-MS interaction. These optical phase control techniques could also be applied in the previous Raman-based scheme [16], where they could mitigate squeezing terms, which were the leading error source; we note that for the SW-MS those terms are inherently suppressed. Our work shows a clear path towards entangling gates with durations comparable to the motional period of the ions (1 s or shorter) at wavelengths that are amenable to largescale chip integration using standard integrated optics [3840] and without the technical challenges of using high-power blue Raman beams [16], pulsed lasers [41, 42] or Rydberg schemes [43].

- The ability for single addressing allows MS gate between two ions in a multi ion chain.
- Also higher intensity at ion can push quadrupole gate time down to speeds where other motional mode inclusion matters (vera).
- Hence explore Fast Optical transition gates at 729 nm in multi ion chain.

3. Experimental Details

The technical complexity of ion trapping experiments may be reduced to solving two problems: Controlling the state of the ion (both internal and motional); and controlling the environment the ion is within. Our Ion trap experiments consist of: an atomic source, a trap, a vacuum system encasing these, external magnetic field coils, and lasers for ionization, cooling, repumping, stateprep, coherent control and readout. As with all ventures in experimental physics, as technologies mature, so too do the capabilities and scope of our apparatus. Here we shall describe both the "old" apparatus, known in short as "Blade", where proof of principle fast gate schemes have been tested, and the new proposed system, known as "FastGates", which solves critical limitations of "Blade" for further exploring fast entanglement and non-adiabatic interactions.

3.1. Ion and Trap

XX Table comparing appropriate dims/freqs/pots of three traps XX

As mentioned, the overall system we desire is a spin coupled to a spring. Our spin in this case being a Hydrogen-like ion, and the spring being the harmonic motion of the

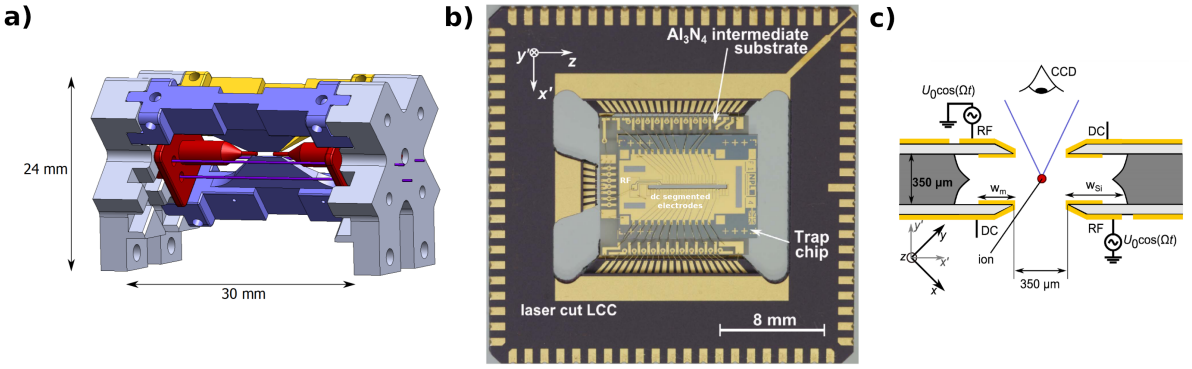

Figure 1. Blade and NPL trap figs from S. R. Woodrow. Linear Paul trap design for high-fidelity , scalable quantum information processing. Master's thesis, University of Oxford, 2015 and [1] K. Choonee, G. Wilpers, and A. G. Sinclair, 'Silicon microfabricated linear segmented ion traps for quantum technologies', in 2017 19th International Conference on Solid-State Sensors, Actuators and Microsystems (TRANSDUCERS), Jun. 2017, pp. 615–618. doi: 10.1109/TRANSDUCERS.2017.7994124.

ions within the trapping potential. The ion traps we use to create such a potential are linear Paul traps, a schematic of such is shown in FigureX. As explained by Earnshaw's theorem, ($\nabla^2 V = 0$), a stable stationary point in 3D can not be realized using a static electric potential, V, as if the potential is confining in 2 dimensions, it will be anticonfining in the third. Therefore to achieve stable trapping a psuedopotential must be utilized. A Paul trap achieves this through an oscillating electric field providing radial confinement and a static field to create axial confinement. There are various popular geometries for realizing a Paul trap: Macro 3D Blade traps; surface traps; and microfabricated segmented 3D traps. A Blade trap, as is used in the "Blade" apparatus, has axial confinement created by DC end caps and radial confinement by supplying an oscillating RF voltage to the blades. In "Blade" the ion endcap distance is 1.15 mm, and ion-blade distance is 0.5 mm. Typical operating frequency for the RF electrodes of the "Blade" trap are 28.0133 MHz leading to an axial ion frequency of 1.860 MHz and radial frequencies of 4.077 MHz and 4.341 MHz.

Recently the surface style linear Paul trap has gained popularity due to the maturity of chip fabrication technologies and the potential route to scalability this offers. In the surface trap, the 3D blade and endcap geometry of the "macro" trap is effectively projected onto a 2D surface. The stable point of such a trap is typically on the order of 50 um from the chip surface. The ease of fabrication of surface traps has allowed the creation of complicated multizone devices with many DC electrodes. These multizone traps enable the shuttling of ions, a requirement for Quantum CCD type architectures. However these benefits come at the cost of trapping potential. Heating of an ion is XXproportionalXX to the ion electrode distance, however so too is the trapping potential. This leads to a compromise of distance... surface trap creates a poor approx of harmonic potential... Therefore weak trap and high heating rates compared to a

macro 3D blade trap. Heating rates of HOA2: axial and radial frequencies...

A microfab 3D trap [See et al and Wilpers 2012], as will be used in the "FastGates" apparatus, brings together the advantages of chip fabrication as well as the low heating rates and high trapping fields of a 3D style trap. This is achieved by a multilayer chip as shown in figureX. The radial trapping is provided by RF rails on opposite diagonals of the slit whilst axial trapping may be realized by DC electrodes on both surfaces. The Ion electrode distance is now of the order 200 um, meaning lower heating, whilst the more optimal 3D geometry allows for a deep potential at this distance (XX 50x surface trap [Guido]). The microfabrication techniques also allow a segmented design suitable for multizone operations and ion shuttling. The 3D confining potential leads to motion of the ions following the Hamiltonian

$$H = \sum_{i=1}^{N} \frac{m}{2}(w_x^2 x_i^2 + w_y^2 y_i^2 + w_z^2 z_i^2 + \frac{|p_i|^2}{m^2}) + \sum_{i=1}^{N} \sum_{j>i} \frac{e^2}{4\pi\epsilon_0 |r_i - r_j|}$$

,

where w_v are the mode frequencies in the three dimensional coordinated. We define z to be the axial direction of the trap and typically assume $w_z \ll w_x,\ w_y$ to allow a 1D ion crystal to lie along the axial direction of the trap. We aim for an axial ion separation of around 5 um which, for ${}^{+}Ca_{40}$ ions means a trapping potential of $w_z \approx 2\pi * 1.6$ MHz. This ion separation was chosen to reduce the cross talk between ions when singly addressed (see section X). We plan for around 5 MHz for our radial frequencies as we will use one such mode for implementing two-qubit entangling gates. This higher frequency is for a few reasons. Firstly, the doppler cooling limit ($\overline{n} = \Gamma/w$, where Γ is the transition linewidth and w is the frequency of the mode being cooled) goes with the reciprocal of the mode frequency and so higher mode frequencies leads to a lower temperature after cooling. Secondly, a higher c.o.m. radial mode leads to better separation of radial modes in a multi-ion crystal which, if we implement the amplitude pulse shaped fast gate scheme described above, can lead to pulse solutions with fewer segments. XX Thirdly, can push to faster gates?

The radial mode frequency is given by w_{rad} equation.
Simulations of the NPL trap, we require an $\Omega_{RF} = XX20$ MHz with a driving amplitude of 180 V to find a solution with axial frequency of 1.6MHz and a radial frequency $w_x = 5$ MHz.

One foreseeable issue with this arrangement becomes apparant when considering the Matthiu equation representing trapping with pseudo-potential. There are areas of stability and instability which can be quantified with the factor q. In Ion traps it has been shown that areas of stability exist for $q < 0.9$, however typical values of q for trapping and cooling ions are considerably smaller. $q = 2 * \sqrt{2} w_{ax}/\Omega_{RF}$. For the proposed plan of 20 MHz RF and 5 MHz radial frequency we would have $q = 0.7$ which although is still stable, may not be able to practically trap from a hot source of ions. Therefore we will likely trap at a lower RF amplitude, lowering the radial frequencies to around 2 MHz where $q < 0.3$ and then ramp up to a tighter trap for efficient doppler

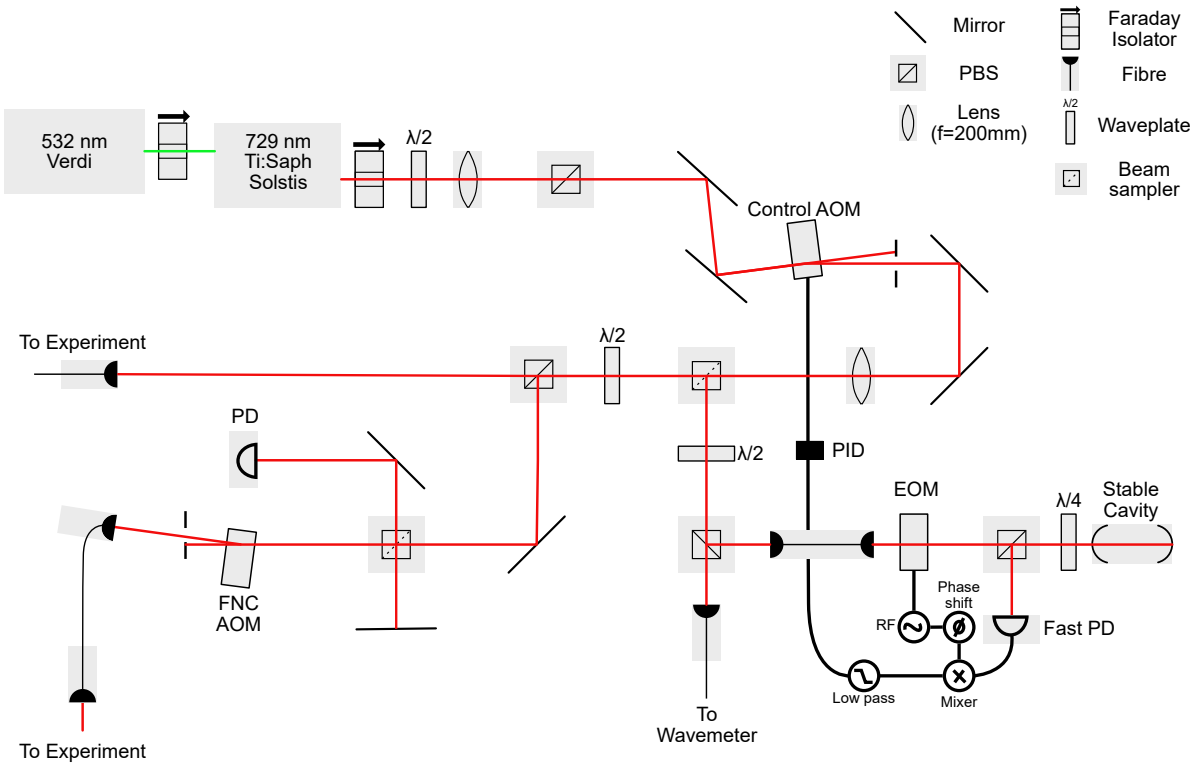

Figure 2. 729 nm system

cooling and fast gate experiments.

Some simulations to find solutions with decent axial and radial modes and figures.

Heating rates... Further, the ion being located within this slit allows for dual high NA optical access (NA = XX), which is an important factor for our proposed single addressing standing wave experiment.

3.2. Laser systems

We have described the trapping of an ion, now we must look at our strategies for manipulating the internal states and collective motion of ion strings. Lasers are a key tool for this as highly localised, strong electric fields amplitudes and gradients can be produced.

First let us consider the $^{40}Ca^{+}$ energy level structure, figure X. The $^{40}Ca^{+}$ has no nuclear spin and is hydrogen like with only one external electron giving a (relatively) simple level structure. An external magnetic field of 5 G is applied to Zeeman split the levels. The relevant laser transitions for our planned ion trap experiment have been marked and their purpose and construction shall be discussed below.

729 nm - Coherent control: As shown in figure X we will use the levels $4S_{1/2}$ to $3D_{5/2}$ with a 729 nm quadrupole transition to define our qubit. Therefore the 729 nm laser is used to implement single and multiqubit gates. We also use this transition, after

doppler cooling, for resolved sideband cooling to step down to near the motional ground state of the ion crystal.

The natural lifetime of the metastable $3D_{5/2}$ is around 1.1 s XrefBarton, giving a favorable fundamental limit of coherence time for our chosen qubit. This natural lifetime leads to a narrow $4S_{1/2}$ to $3D_{5/2}$ transition linewidth $\Gamma < 1$ Hz, and so demands the use of a narrow linewidth laser. Further, we require a high light intensity at the ion to drive sideband transitions due to a low Lamb-Dicke factor for 729 transition, $\eta \approx 0.05$. Pumped Ti:Saph laser systems have been shown to be both relatively high power and narrow linewidth, making them suitable for our experiment.

We pump an M2 Solstis Ti:Saph with 15 W of 532 nm light from a Verdi system to produce around 4W of 729 nm light. A schematic of the 729 nm system being built is shown in figure X. The frequency is stabilized by the Pound-Drever-Hall (PDH) technique with a high finesse cavity. PDH locking requires taking the laser light and applying two sidebands via an electro-optical modulator (EOM). This phase modulated light is then directed onto a stable cavity and a reflected signal is directed onto a fast photodetector. The reflection from the cavity consists of the interference between the carrier and the sidebands which have been respectively altered by the cavity transfer function. The photodetector signal is mixed down with the same oscillator signal as provided to the EOM but delayed by some phase, and finally low pass filtered to produce a signal for use as the error signal in the servo loop. This error gives a measure for how far the carrier frequency is from the stable cavity resonant frequency and is used for feedback onto the control AOM situated after the Solstis.

Some of the 729 nm light is picked off and sent to a wavemeter to monitor the frequency however the majority is coupled to two output fibres for our experiment and another within the group. We require fibre noise cancellation as we transport the 729 light from a laser lab to the trapping lab by a 10 m single mode polarization maintaining fibre and must ensure no phase noise is introduced.

Trial of Verdi C unsuccesful so far not achieving stable lasing with solstis. Improvements over Blade: - 729 more convenient Ti:Saph freq -> Higher power, low noise - access parallel to radial mode, Blade is 45 deg -> High Lamb Dicke factor - 729 more convenient for putting in fibre -> low charging

393 and 432 - PI Two step photoionization for isotope selectivity.

397 - Doppler Cooling, Fluorescent readout Dipole transition for Doppler cooling as want fast scattering. Also want higher freq light for more momentum transfer. Fluor read out so that |0> bright and |1> dark.

854 and 866 - Repumping as branching ratio from P to S and D. So during cooling and readout we lose population to these levels.

All of the above systems are Toptica Diode lasers coupled to a cavity for PDH locking.

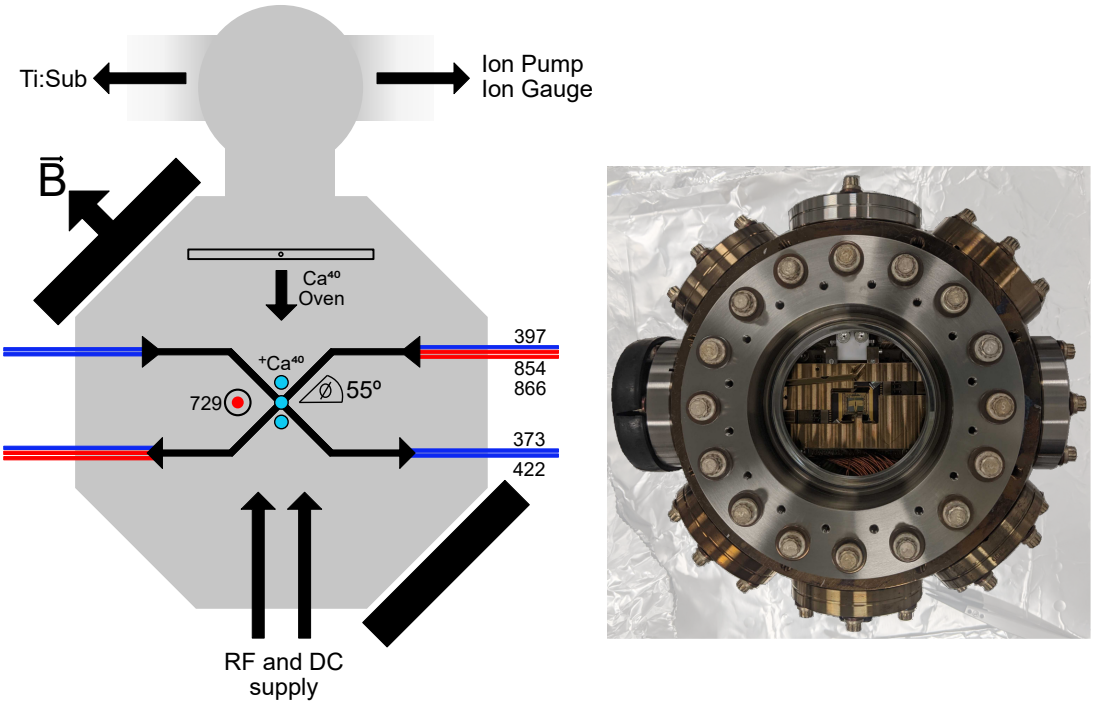

Figure 3. Vacuum can

3.3. Inside the vacuum

Here we shall describe the instrumentation required, and being constructed, for decouping the ion from any unwanted external environments. Our primary tools for this are working under Ultra High Vacuum (UHV) and surrounding the vacuum system with electromagnetic shielding. Inside the vacuum system we aim for a residual pressure of less than 10^{-11} mbar. To reach this low a pressure, we must take care in material choice and thoroughly clean and bake all material within the vacuum system (a useful summary of tactics can be found in [ref]).

A schematic of the vacuum system can be seen in figure X. The system consists of an octagonal experimental chamber connected to an Ion pump, Ion Gauge and Ti:Sub pump. For optical access we have Dual CF100 viewports coated for 397 nm and 729 nm as well as two CF40 viewports coated for 397 nm, 422 nm, 729 nm, 854 nm and 866 nm.

As discussed above, our ion will be located within a slit of the NPL trap and so there is no visibility of the ions from the side CF40 viewports. We therefore are using in vacuum prisms to direct the light onto the ions at XX degrees.

We use an electrical feedthrough on a CF40 flange to supply our trap chip with both DC and RF voltages. As the DC cables run within close proximity to the RF

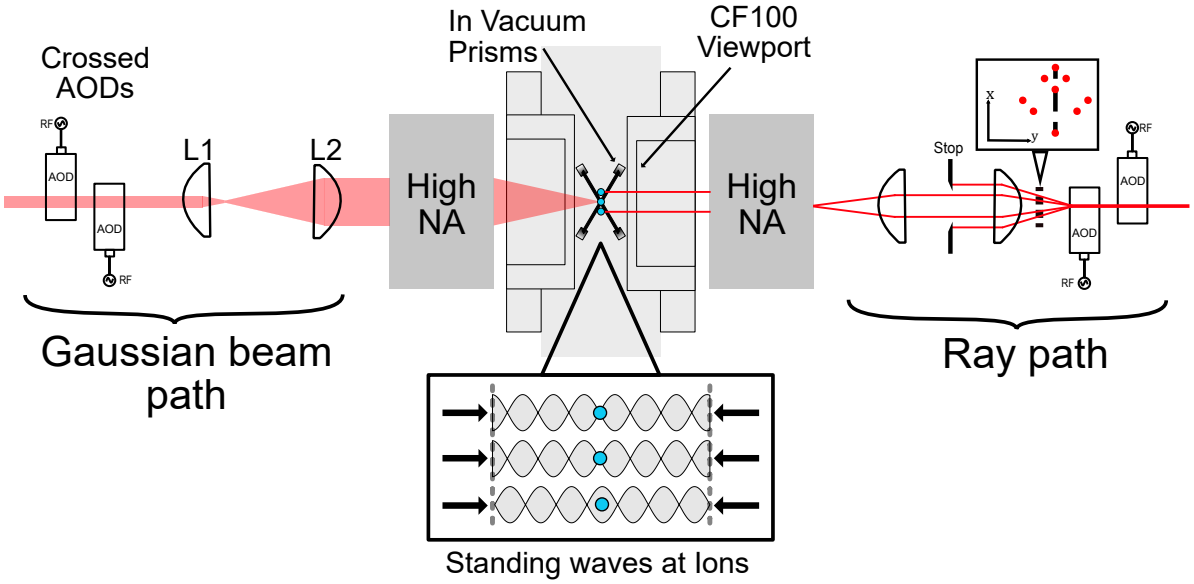

Figure 4. Single addressing system

supply, electrical pick up is a potential issue within our DC lines. We mitigate this through a low pass filter board within close proximity of the trap chip. We implement a "trap stack", seen in figure X, within the vacuum chamber consisting of the trap chip, the outer chip carrier, an interposer, and the filter PCB.

$^{+}Ca_{40}$ was chosen for zero nuclear spin and therefore simple energy level structure. However we now cannot utilize hyperfine structure to find "clock" qubits which are insensitive to magnetic field fluctuations and must instead remove magnetic field noise from the environment. To suppress this noise we place the vacuum chamber within a box constructed from two layers of 3mm thick MuMetal [ref]. The shielding was shown to suppress the background field by a factor of 500 at its center.

3.4. Single Addressing

729 High NA (0.6) lens we can achieve waist radius of < 1 um. With our axial trap freq of XXX we get ion spacing of 5um. Using AOD system we can traverse this ion chain. Description of lens system from AOD to ions. Description on the mechanism on how AOD works (this is the same as an AOM). Comparison between this and a fixed waveguide array. What equations we need to find number of resolvable spots of the AOD system. AOD have extra programmable control than waveguides which is excellent as we are in an exploratory regime where we may want to alter ion spacing/Dont want to use quartic potentials to make ions evenly spaced. We will use a crossed AOD design so that we have no overall frequency shift as we scan along the ion chain. Compact design to fit beam path within MuMetal box. We want to create single addressing standing wave so must consider stabilization technique from AOD. There is minimal path length differece compared to waveguide which is ideal as we can stabilise at some

central frequency and should be stable at all ion locations. Quick calculation to look at path length diff in wavlengths between two extrema points on the ion chain. Note that this will give some fixed relationship between the two beams if we assume that the small seperation of beams paths is negligible (air density and current in close proximity should be related). Using two RF freq so that we can address two ions at the same time. Initially looking at this we see that supplying two freqs and amplifying we dont have crazy cross term amplitudes. However addressing multiple ions at the same time comes at the cost of photon freq cross terms i.e. spots that we dont want that are off plane to our ions. This has two bad effects: Can get crosstalk to other ions on the chain and lose power in our 729 system. First effect we can mitigate by putting AOD at a $>$ 45 deg angle (60 deg?) this pushes the unwanted spots further from the chain. (sep to ion is sqrt2/2 when at 45 deg). There is no easy way to mitigate the power loss as two freq photons are barely distinguishable (maybe look again at the two wavelength design aods). So this may limit us to only addressing 2 or three ions at a time and using a global addressing system through the prisms if all ions need to be addressed. Quick power calculation though means we still have XXmW at each ion with an intensity of XX which could drive CNulled gates at a speed of X.

subtitle FastGates Apparatus

*This has been (to be) incorportated into the above section.

Here we describe the design of the new "FastGates" system which is tailored for the exploration of fast, non-adiabatic entangling gates. Figure X shows a schematic of the vacuum can of "FastGates" with the addressing directions and magnetic field highlighted. Ca40 was chosen for initial experiments due to its simple energy level structure, figure X, without hyperfine levels and with the option for a quadrupole qubit between the S and D levels. An external magnetic field of 5G is applied to define our Zeeman sublevels, this low field will not allow state selective addressing by frequency, however allows for polarization selective addressing. *** Check if 729 will actually have linewidth for frequency addressing? *** The isotope having 0 nuclear spin and hence no hyperfine levels greatly simplifies control schemes however precludes the option of using magnetically insensitive "clock" qubits. To ensure we do not greatly limit coherence time of our quadrupole transition we use a MuMetal enclosure to suppress stray environmental magnetic fields.

4. Outlook

Current state of building up apparatus. Immediate next steps. Proposed first experiments? GANNT diagram?